Acta Mech. Sin. (2011) 27(5):738–748
DOI 10.1007/s10409-011-0496-y

RESEARCH PAPER

Finite element analysis of 2D SMA beam bending

Shi-Bin Yang · Min Xu

Received: 12 May 2010 / Revised: 28 October 2010 / Accepted: 27 April 2011

Abstract A thermomechanical model of a shape memory alloy beam bending under tip force loading is implemented in finite element codes. The constitutive model is a one dimensional model which is based on free energy and motivated by statistical thermodynamics. The particular focus of this paper is on the aspects of finite element modeling and simulation of the inhomogeneous beam bending problem. This paper extends previous work which is based on the small deformation Euler–Bernoulli beam theory and by treating an SMA beam as consisting of multi-layers in a two-dimensional model. The flux terms are involved in the heat transfer equation. The simulations can represent both shape memory effect and super-elastic behavior. Different thermal boundary condition effect and load rate effect can also be captured.

Keywords Shape memory alloy · SMA cantilever beam · Thermomechanical · Martensitic transformation · Finite element analysis

1 Introduction

Shape memory alloys (SMAs) exhibit two unique properties, the shape memory effect and pseudo-elasticity. The shape memory effect (SME) is the material's ability to recover the large residual deformation generated at low temperatures by moderate increases in temperature. The pseudo-elasticity (super-elasticity) refers to the ability to generate and recover large deformations during loading and unloading cycles at higher temperatures. The underlying mechanism is a reversible martensitic transformation between solid-state phases. The transformation can be triggered by changes in temperature and/or by changes in stress due to the strong thermomechanical coupling. SMAs also exhibit nonlinear hysteresis behavior.

SMAs have found widespread use in a number of different areas. Due to their capability of large actuation force and displacement, SMAs have become a promising unconventional actuator candidate during the last two decades. More recently, SMAs have also been fabricated as micro-actuators using thin film techniques [1]. The large surface to volume ratio of SMA thin films allows fast cooling compared to bulk SMA materials. This increases the bandwidth of the SMA actuator dramatically. Some interesting applications include micro-grippers [2], micro-pumps [3] and micro-cantilever switches [4]. Kohl et al. [5] developed a novel actuation mechanism using a thin film ferromagnetic NiMnGa micro-actuator which makes use of the combination of its conventional SMA properties and ferromagnetism. A novel silicon cantilever beam device actuated by Ti–Ni SMA films was developed [6]. This device was used in a microelectromechanical system (MEMS) probe card that provided a relatively large contact force between the probe and electrode pad in spite of its minute size, and also provided additional contact force by the shape memory effect of the Ti–Ni film arising from Joule heating. To facilitate the development of these new devices, an efficient continuum model and computational tool such as finite element method has to be used.

Proposed models for SMAs in the literature are quite numerous. Early efforts go back to Tanaka [7]. The model uses the fraction of martensite as an internal variable and gives a phenomenological equation of state for its dependence on stress and temperature in the form of an exponential function. Liang and Rogers [8] later modified the model

S.-B. Yang (✉)
Aircraft Airworthiness Certification Research Center,
Civil Aviation University of China,
300300 Tianjin, China
e-mail: yshb2003@yahoo.com.cn

S.-B. Yang · M. Xu
Department of Astronautics,
Northwestern Polytechnical University,
710072 Xi'an, China

by using a cosine law for the martensite fraction. Ginzbug-Landau's model was developed to simulate microstructure evolution [9], atomic-scale models to predict crystal structures [10], and even quantum-mechanical models to evaluate the relative stability of different crystal structures [11]. A noticeable model has been developed by Ivshin and Pence [12]. The model takes thermodynamics into consideration. Despite a certain lack of physical reasoning, the model appears to be quite powerful with respect to the simulation of SMA actuator behavior. It includes an energy balance with contributions from convective heat exchange, latent heat and external heat sources, and a range of pseudo-elastic behavior from isothermal to adiabatic in a convective environment are displayed in Ref. [12].

These rather complex thermomechanical interactions can present serious difficulties to the application engineer who wishes to design novel devices or new composite materials with SMA constituents, and the phenomena have important repercussions on the performance, reliability, and controllability of the material as passive or active constituents. More and more researchers have concentrated on thermomechanical coupling model and simulation [13–18].

One of the latest models for SMA wires is developed by Shaw [19]. The model is capable of simulating both superelastic and shape memory behaviors of SMAs. A coupled thermomechanical boundary value problem and constitutive relations were derived for a 1D SMA element. Mechanical equilibrium and heat equations were derived with strain gradient effects. Later, Iadicola and Shaw [20] extended the above model to investigate the trends of localized nucleation and propagation phenomena for a wider range of loading rates and ambient thermal conditions. Chang and Shaw [21] implemented their thermomechanical model for an SMA wire under uniaxial loading in a finite element framework and captured the temperature distribution by representative infrared image. The model is then used to simulate a simple SMA actuator device, and its performance is assessed for different thermal boundary conditions. Recently, Shaw and Churchill [22] reduced the system of partial differential equations for an SMA/bias spring actuator to a nonlinear, first-order, ordinary differential equation. They demonstrated a simple model of a prototype SMA wire/bias spring actuator that admits analytical solutions for time dependent behavior.

Another model that has recently been applied to SMA applications has originally been developed by Achenbach and Müller [23], Achenbach [24] and Seelecke and Müller [25]. It uses ideas from statistical thermodynamics and describes the evolution of two martensite fractions which is based on the theory of thermally activated processes. The attractiveness of the model is based on the fact that the complete load-temperature-dependent hysteretic behavior of SMAs is derived from the energy function alone without any additional loading/unloading criteria. The model can represent both shape memory effect and super-elasticity of SMA materials. A very limited number of material parameters are used to construct the free energy which can be identified from only two tensile experiments conducted at two different temperatures. Together with a convenient mathematical structure in the form of an ODE system, allowing for robust numerical integration, these features make the model an attractive candidate for the simulation of SMA actuators and their control behavior.

Using the above constitutive models, most of the simulation work is on a 1 dimensional SMA wire under uniaxial loading. Recently, there is also some work on SMA beam or thin film simulation and analysis. A multi-axial pseudo-elastic model was implemented to predict the dynamic behavior of shape memory alloys in Ref. [26] based on a phenomenological model (Rl model). Cantilever SMA beams with variable cross section were discussed in Ref. [27]. Our previous work [28] was to treat the beam as multi-layers based on the small deformation Euler–Bernoulli beam theory. Each layer is governed by a 1D free energy SMA model. However, in reality, the latent heat transfers in every direction, which will affect the phase transformation in adjacent domains. As a result, the beam or thin film thermomechanical coupling effect has to be modeled as two dimensional at least.

The objective is to implement the thermomechanical 2D SMA beam in a finite element framework. Such a 1D thermomechanical constitutive model which is based on free energy will be introduced. Heat transfer, convection and latent heat will be considered for the SMA beam which can capture the non-uniform strain and temperature distribution. The implementation of the 2D model in COMSOL will be illustrated. A series of cantilever beam simulations will be conducted. Shape memory effect, super-elastic behavior, load rate effect, different thermal boundary conditions, non-uniform temperature and strain distribution, as well as developing phase transformation will be discussed. This work can provide an efficient calculation tool for SMA beams, predicting the performance, and for initial design of the adaptive structure which is integrated in such SMA beams.

2 1D free energy SMA model

In this section, the Müller–Achenbach model in the version which was proposed by Seelecke [25] is described. It uses ideas from statistical thermodynamics and describes the evolution of two martensite phase fractions based on the theory of thermally activated processes. Motivated by crystallographic observations, a mesoscopic lattice layer is treated as the basic element of the model. Under uniaxial loading, apart from austenite A, there are only two martensitic variants, denoted as M_+ and M_-, and their phase fractions are denoted as x_A, x_+ and x_-, respectively, satisfying the following relationship

$$x_{\mathrm{A}} + x_{+} + x_{-} = 1. \tag{1}$$

The macroscopic strain in a shape memory alloy may be written as the weighted sum of the strains in the individual phases as follows

$$\varepsilon = x_{\mathrm{A}}\langle\varepsilon_{\mathrm{A}}\rangle + x_{+}\langle\varepsilon_{+}\rangle + x_{-}\langle\varepsilon_{-}\rangle, \tag{2}$$

where $\langle\varepsilon_{\mathrm{A}}\rangle$, $\langle\varepsilon_{+}\rangle$ and $\langle\varepsilon_{-}\rangle$ are the average strains in each phase, which can be calculated according to Boltzmann statistics. Assuming the Gibbs free energy function G to be a multi-parabolic function, we can write the average strains as

$$\langle\varepsilon_{\mathrm{A}}\rangle = \frac{\int_{-\varepsilon_{\mathrm{A}}}^{\varepsilon_{\mathrm{A}}} \varepsilon \mathrm{e}^{-G(\varepsilon,\sigma,T)V_{\mathrm{D}}/kT}\mathrm{d}\varepsilon}{\int_{-\varepsilon_{\mathrm{A}}}^{\varepsilon_{\mathrm{A}}} \mathrm{e}^{-G(\varepsilon,\sigma,T)V_{\mathrm{D}}/kT}\mathrm{d}\varepsilon} \approx \frac{\sigma}{E_{\mathrm{A}}}, \tag{3}$$

$$\langle\varepsilon_{+}\rangle = \frac{\int_{\varepsilon_{\mathrm{M}}}^{\infty} \varepsilon \mathrm{e}^{-G(\varepsilon,\sigma,T)V_{\mathrm{D}}/kT}\mathrm{d}\varepsilon}{\int_{\varepsilon_{\mathrm{M}}}^{\infty} \mathrm{e}^{-G(\varepsilon,\sigma,T)V_{\mathrm{D}}/kT}\mathrm{d}\varepsilon} \approx \frac{\sigma}{E_{\mathrm{M}}} + \varepsilon_{\mathrm{T}}, \tag{4}$$

$$\langle\varepsilon_{-}\rangle = \frac{\int_{-\infty}^{-\varepsilon_{\mathrm{M}}} \varepsilon \mathrm{e}^{-G(\varepsilon,\sigma,T)V_{\mathrm{D}}/kT}\mathrm{d}\varepsilon}{\int_{-\infty}^{-\varepsilon_{\mathrm{M}}} \varepsilon \mathrm{e}^{-G(\varepsilon,\sigma,T)V_{\mathrm{D}}/kT}\mathrm{d}\varepsilon} \approx \frac{\sigma}{E_{\mathrm{M}}} - \varepsilon_{\mathrm{T}}, \tag{5}$$

where V_{D} is the representative volume and k is the Boltzmann constant. From Eqs. (2)–(5), we can derive the explicit stress–strain relation as

$$\sigma(\varepsilon) = \frac{E_{\mathrm{M}}[\varepsilon - (x_{+} - x_{-})\varepsilon_{\mathrm{T}}]}{x_{+} + x_{-} + x_{\mathrm{A}}E_{\mathrm{M}}/E_{\mathrm{A}}}. \tag{6}$$

This is the constitutive stress–strain equation that will be used in the finite element implementation. The evolution of the phase fractions x_{α}, $\alpha = \{\mathrm{A}, +, -\}$ is governed by the rate laws

$$\begin{aligned} \dot{x}_{+} &= -x_{+}p^{+\mathrm{A}} + x_{\mathrm{A}}p^{\mathrm{A}+}, \\ \dot{x}_{-} &= -x_{-}p^{-\mathrm{A}} + x_{\mathrm{A}}p^{\mathrm{A}-}, \end{aligned} \tag{7}$$

and from Eq. (1), the phase fraction of austenite x_{A} is given as

$$x_{\mathrm{A}} = 1 - x_{+} - x_{-}. \tag{8}$$

The rate of change of $x_{\pm}$ is the sum of a loss that is due to layers jumping from the $\mathrm{M}_{\pm}$ phase to the A phase, and a gain that is due to layers jumping from the A phase to the $\mathrm{M}_{\pm}$ phase. The quantities $p^{\alpha\beta}$ in Eq. (7) are called transition probabilities which are computed as the product of the probability of achieving the energy required to overcome the energy barrier between neighboring wells and the frequency at which jumps are attempted. They can be expressed explicitly as

$$\begin{aligned} p^{\pm\mathrm{A}}(\sigma,T) &= \frac{1}{\tau}\frac{\mathrm{e}^{-\frac{V_{\mathrm{D}}}{2E_{\mathrm{M}}kT}(\sigma_{\mathrm{M}}\mp\sigma)^2}}{\mathrm{erf}\Big[\sqrt{\frac{V_{\mathrm{D}}}{2E_{\mathrm{M}}kT}}(\sigma_{\mathrm{M}}\mp\sigma)\Big]}, \\ p^{\pm\mathrm{A}}(\sigma,T) &= \frac{1}{\tau}\Big[\mathrm{e}^{-\frac{V_{\mathrm{D}}}{2E_{\mathrm{A}}kT}(\sigma_{\mathrm{A}}\mp\sigma)^2}\Big]\Big/\Big\{\mathrm{erf}\Big[\sqrt{\frac{V_{\mathrm{D}}}{2E_{\mathrm{A}}kT}}(\sigma_{\mathrm{A}}+\sigma)\Big] \\ &\quad +\mathrm{erf}\Big[\sqrt{\frac{V_{\mathrm{D}}}{2E_{\mathrm{A}}kT}}(\sigma_{\mathrm{A}}-\sigma)\Big]\Big\}, \end{aligned} \tag{9}$$

where τ is the relaxation time for the process, σ_{A} is a loading stress at which a phase transition from austenite to martensite M_{+} begins, and σ_{M} is an unloading stress at which a phase transition from M_{+} to austenite begins. The transition probabilities are functions of stress σ and temperature T.

SMA actuators are typically driven by Joule heating and convective cooling. Coupled with the mechanical loading, the temperature changes trigger the phase transformations between martensite and austenite and consequently generate the deformation of the SMA actuator. Assuming uniform temperature changes throughout the SMA material, the heat transfer equation reads [23]

$$\rho c\dot{T} = -\alpha S_{\mathrm{V}}(T - T_0) + j(t) - (h_{\mathrm{M}+} - h_{\mathrm{A}})\dot{x}_{+} - (h_{\mathrm{M}-} - h_{\mathrm{A}})\dot{x}_{-}, \tag{10}$$

where ρ is the density and c is the specific heat. We assume the same specific heats for austenite and martensite. The first term on the right hand side of Eq. (10) is the heat convection to the environment with temperature T_0. The heat transfer coefficient between the SMA actuator surface and its surrounding environment is denoted by α and the surface area to volume ratio is S_V. The Joule heating is denoted by $j(t)$. The last two terms on the right hand side of Eq. (10) account for the rate-dependent heat generation and absorption due to phase transformations, where $h_{\mathrm{M}\pm} - h_{\mathrm{A}}$ are called the latent heats of the transformations and given as

$$h_{\mathrm{M}\pm} - h_{\mathrm{A}} = -\frac{\sigma^2}{2}\frac{E_{\mathrm{M}} - E_{\mathrm{A}}}{E_{\mathrm{M}}E_{\mathrm{A}}} \mp \sigma\varepsilon_{\mathrm{T}} - \Delta u, \tag{11}$$

where Δu is given in Ref. [25] along with a detailed discussion about the latent heats.

The model can be summarized as the stress–strain relation equation (6) complemented by a system of nonlinear ODEs, which govern the evolution of the martensite phase fractions (7) and the temperature (10)

$$\varepsilon = x_{\mathrm{A}}\frac{\sigma}{E_{\mathrm{A}}} + x_{+}\Big(\frac{\sigma}{E_{\mathrm{M}}} - \varepsilon_{\mathrm{T}}\Big) + x_{-}\Big(\frac{\sigma}{E_{\mathrm{M}}} + \varepsilon_{\mathrm{T}}\Big), \tag{12}$$

$$\begin{aligned} \dot{x}_{+} &= -x_{+}p^{+\mathrm{A}} + x_{\mathrm{A}}p^{\mathrm{A}+}, \\ \dot{x}_{-} &= -x_{-}p^{-\mathrm{A}} + x_{\mathrm{A}}p^{\mathrm{A}-}, \end{aligned} \tag{13}$$

$$\rho c\dot{T} = -\alpha S_{\mathrm{V}}(T - T_0) + j(t) - (h_{\mathrm{M}+} - h_{\mathrm{A}})\dot{x}_{+} - (h_{\mathrm{M}-} - h_{\mathrm{A}})\dot{x}_{-}, \tag{14}$$

where the transition probabilities $p^{\alpha\beta}(\sigma,T)$ are given in Eq. (9). For given applied stress $\sigma(t)$ and Joule heating $j(t)$, we can evaluate phase fraction $x_{\alpha}(t)$ and temperature $T(t)$ by

integrating the ODEs of Eqs. (13) and (14) simultaneously, and then calculate the resulting strain $\varepsilon(t)$ from Eq. (12). Alternatively, prescribing strain $\varepsilon(t)$ and Joule heating $j(t)$, we can calculate $x_\alpha(t)$, $T(t)$ and $\sigma(t)$. Initial conditions of phase fractions $x_+(0)$, $x_-(0)$ and temperature $T(0)$ need to be given to start the integration.

3 Thermo-mechanical problems of the SMA beam

The behavior of SMA materials is characterized by strong thermo-mechanical coupling due to the rate-dependent latent heats released and absorbed during austenite–martensite phase transformations. Unlike SMA wire, the SMA beam sustains moment and force. If the loads are in plane, the beam can be modeled as 2 dimensional which assumes that it is homogeneous out of the plane. The heat transfer equation given in Eq. (10) is under the assumption of uniform temperature throughout the SMA devices. In reality, however, due to the factors such as non-homogeneous geometry, boundary conditions, temperature dependent resistivity, localized self-heating or self-cooling due to latent heat effects, the temperature distribution in the SMA beam is non-homogeneous. A space dependent nonlinear transient thermo-mechanical coupled problem has to be solved. Heat will not only be conducted in the length direction, but also be conducted in the height (perpendicular) direction.

According to the first law of thermodynamics, we re-derive the 2D heat transfer equation by including heat conduction as

$$\rho c\frac{\partial T}{\partial t} - \frac{\partial}{\partial x}\Big(\lambda\frac{\partial T}{\partial x}\Big) - \frac{\partial}{\partial y}\Big(\lambda\frac{\partial T}{\partial y}\Big) = j(t) - (h_{\mathrm{M}+} - h_{\mathrm{A}})\dot{x}_+ - (h_{\mathrm{M}-} - h_{\mathrm{A}})\dot{x}_-, \tag{15}$$

where the second and third term on the left hand side of Eq. (15) is the gradient of the heat flow and λ is the heat conductivity. The first term on the right hand side of Eq. (10) is not shown in Eq. (15) because the heat convection between the materials and circumstance becomes the boundary condition in the 2D problem. The term $j(x,t)$ represents Joule heating density.

4 Implementation of 2D SMA beam

In this section, we will derive the beam's mechanical equations based on the small deformation Euler–Bernoulli beam theory. In consequence, we will implement the 2D SMA beam in FE package.

4.1 Basic beam equations

For the cantilever beam which is shown in Fig. 1, the force equilibrium equation can be derived as

$$\frac{\partial Q}{\partial x} = -q(x), \tag{16}$$

with the shear force $Q(x)$ and the continuous loading $q(x)$. Moment equilibrium results in

$$\frac{\partial M}{\partial x} = Q, \tag{17}$$

with the cross section moment $M(x)$, which is the resultant of the stresses normal to the cross section and which can be integrated as

$$M(x) = -b\int_{-h/2}^{h/2} y\sigma(x,y)\mathrm{d}y. \tag{18}$$

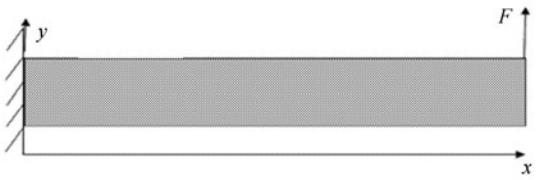

Fig. 1 Cantilever beam

The stress–strain relation is the same as the SMA wire except that the degree of freedom becomes two.

$$\sigma(x,y) = \frac{E_{\mathrm{M}}\{\varepsilon(x,y) - [x_+(x,y) - x_-(x,y)]\varepsilon_{\mathrm{T}}\}}{x_+(x,y) + x_-(x,y) + \dfrac{E_{\mathrm{M}}}{E_{\mathrm{A}}}x_{\mathrm{A}}(x,y)}. \tag{19}$$

But according to the kinematic assumptions of the Euler–Bernoulli Beam theory, the strain is now a function of position y. It is calculated as

$$\varepsilon(x,y) = -y\frac{\partial\theta}{\partial x}, \tag{20}$$

with the deflection angle $\theta(x)$ following from the transverse deflection $W(x)$ of the beam as

$$\frac{\partial W}{\partial x} = \theta. \tag{21}$$

From Eqs. (18)–(20), the cross section moment can be derived as

$$M(x) = -b\int_{-h/2}^{h/2} y\sigma(x,y)\mathrm{d}y = \beta\frac{\partial\theta}{\partial x} + \gamma, \tag{22}$$

where

$$\beta = b\int_{-h/2}^{h/2} y^2\frac{E_{\mathrm{M}}}{x_+(x,y) + x_-(x,y) + \dfrac{E_{\mathrm{M}}}{E_{\mathrm{A}}}x_{\mathrm{A}}(x,y)}\mathrm{d}y,$$
$$\gamma = b\int_{-h/2}^{h/2} y\frac{E_{\mathrm{M}}\{[x_+(x,y) - x_-(x,y)]\varepsilon_{\mathrm{T}}\}}{x_+(x,y) + x_-(x,y) + \dfrac{E_{\mathrm{M}}}{E_{\mathrm{A}}}x_{\mathrm{A}}(x,y)}\mathrm{d}y. \tag{23}$$

4.2 Implementation in COMSOL

Here, we re-write the SMA equations (13) and (15) in PDE mode which can be implemented in COMSOL. We hence treat the phase fractions x_+, x_- as well as temperature T as additional solution variables, $U = [x_+ \quad x_- \quad T]^{\mathrm{T}}$ and write the PDE system as following form

$$\boldsymbol{d}_\alpha \frac{\partial \boldsymbol{U}}{\partial t} + \nabla \cdot \boldsymbol{\Gamma} = \boldsymbol{F}, \tag{24}$$

with

$$\boldsymbol{d}_\alpha = \begin{bmatrix} 1 & 0 & 0 \\ 0 & 1 & 0 \\ (h_{\mathrm{M}+} - h_{\mathrm{A}}) & (h_{\mathrm{M}-} - h_{\mathrm{A}}) & \rho c \end{bmatrix}, \tag{25}$$

$$\boldsymbol{\Gamma} = \begin{bmatrix} 0 & 0 \\ 0 & 0 \\ -\lambda \dfrac{\partial T}{\partial x} & -\lambda \dfrac{\partial T}{\partial y} \end{bmatrix}, \tag{26}$$

$$\boldsymbol{F} = \begin{bmatrix} -x_+ p^{+\mathrm{A}}(\sigma, T) + (1 - x_+ - x_-) p^{\mathrm{A}+}(\sigma, T) \\ -x_- p^{-\mathrm{A}}(\sigma, T) + (1 - x_+ - x_-) p^{\mathrm{A}-}(\sigma, T) \\ j(t) \end{bmatrix}. \tag{27}$$

Using the shear force $Q(x)$, moment $M(x)$, deflection angle $\theta(x)$ and deflection $W(x)$ as the solution variables $\boldsymbol{U} = [Q \quad M \quad \theta \quad W]^{\mathrm{T}}$. The beam equations (16), (17), (21) and (22) can also be written in PDE form in the same way

$$\boldsymbol{d}_\alpha = [0]_{4\times 4}, \tag{28}$$

$$\boldsymbol{\Gamma} = [Q \quad M \quad \theta \quad W]^{\mathrm{T}}, \tag{29}$$

$$\boldsymbol{F} = \begin{bmatrix} -q(x) \\ Q \\ \dfrac{M - \gamma}{\beta} \\ \theta \end{bmatrix}. \tag{30}$$

From the above, we know that the variables in the SMA model as well as stress and strain are 2 dimensional. However, the variables in the beam equations are 1D . The trick of the implementation is how to connect the solution variables in different dimensions. The implementation of the 2D SMA beam in COMSOL is illustrated step by step in the following part.

Step 1 Define two geometries in one model. One is the 2D beam geometry which is the domain to define 2D variables. The other is the 1D line with beam's length which will have 1D variables put on.

Step 2 Define general PDE applications on these two geometries according to Eqs. (24)–(30).

Step 3 Define a projection variable Moment in the 2D beam application. It will implement the integration as

$$M(x) = b \int_{-h/2}^{h/2} y\sigma(x, y)\mathrm{d}y,$$

which can project the 2D variable stress to 1D variable moment. At the same time, define an extrusion variable which can extrude the 1D variable θ to 2D variable strain.

$$\varepsilon(x, y) = -y \frac{\partial \theta}{\partial x}.$$

Step 4 Create elements for the domains. The areas which have a larger gradient should have finer elements. In this case, a cantilever under concentrated bending force as shown in Fig. 1, the phase transformation will occur at the top and bottom area in the clamped end. So these areas need to have the finest elements.

5 Simulation and discussion

The geometry parameters of the SMA cantilever beam with rectangular cross section and SMA material parameters are shown in Table 1. Due to the latent heat super-elastic behavior is much more obvious than that in the quasi-plastic behavior, we here study the shape memory effect of the SMA beam bending under isothermal assumptions and super-elasticity of the SMA beam bending under different thermal boundary conditions and load rate effect.

Table 1 Simulation parameters

SMA	Parameters values
Length L/mm	100
Width b/mm	15
Height h/mm	10
E_{A}/GPa	71.1
E_{M}/GPa	30.9
ε_T	0.044
V_{D}/m^3	5×10^{-23}
τ/s	0.01
$\sigma_{\mathrm{A}}(T_U = 353\,\mathrm{K})$/MPa	663.16
$\sigma_{\mathrm{A}}(T_L = 323\,\mathrm{K})$/MPa	431.58
$\Delta\sigma$/MPa	295

5.1 Shape memory effect

An important property of SMA materials is the shape memory effect (SME), which is due to the temperature-induced

phase transformations in SMA materials. Under isothermal assumptions, we study the SME of the inhomogeneous quasi-static SMA beam bending. Figures 2 and 3 illustrate the SME of the beam bending under thermomechanical loadings. First, under constant low temperature $T = 253\,\mathrm{K}$, where martensite states are stable, the simulation starts with $x_+ = x_- = 0.5$.

Figure 2 presents the time histories of the applied force, temperature, and corresponding force–temperature–displacement diagram. From the contour plots of the stress, strain and phase fractions shown in Fig. 3, we can see that, due to the non-uniform stress distribution throughout the SMA beam, the phase transformation starts from the outer layer at the clamped end with the maximum stress and propagates through the thickness and along the length of the beam with increasing loading. The section below the neutral axis is subjected to tensile stresses and phase transformation occurs from martensite $M_\pm$ to M_+. The section above the neutral axis is subjected to compression stress and transforms from martensite $M_\pm$ to M_-. After the unloading is completed, there is a residual strain distribution, which contributes to the global residual deformation of the SMA beam. The stresses in each cross–section are re-distributed to satisfy zero cross–section moment, which generates a complex residual stress distribution. Then under zero mechanical loading and after being heated up to a high temperature, the SMA material transforms from martensite M to austenite A and recovers to the original undeformed shape. And after being cooled down to a low temperature, the austenite A becomes unstable and transforms to martensite $M_\pm$.

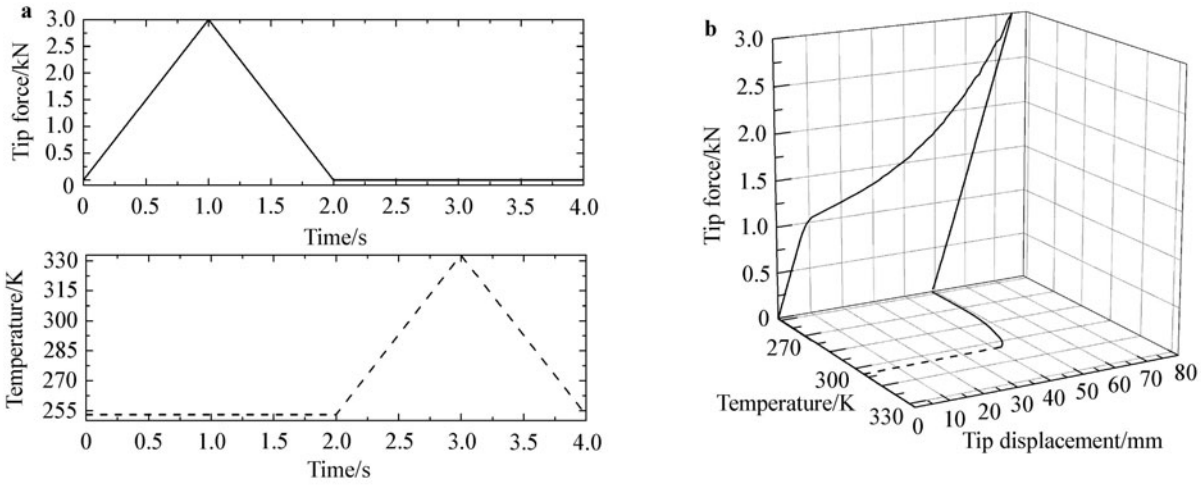

Fig. 2 Shape memory effect of SMA beam bending: **a** Applied tip force and temperature; **b** Shape memory effect

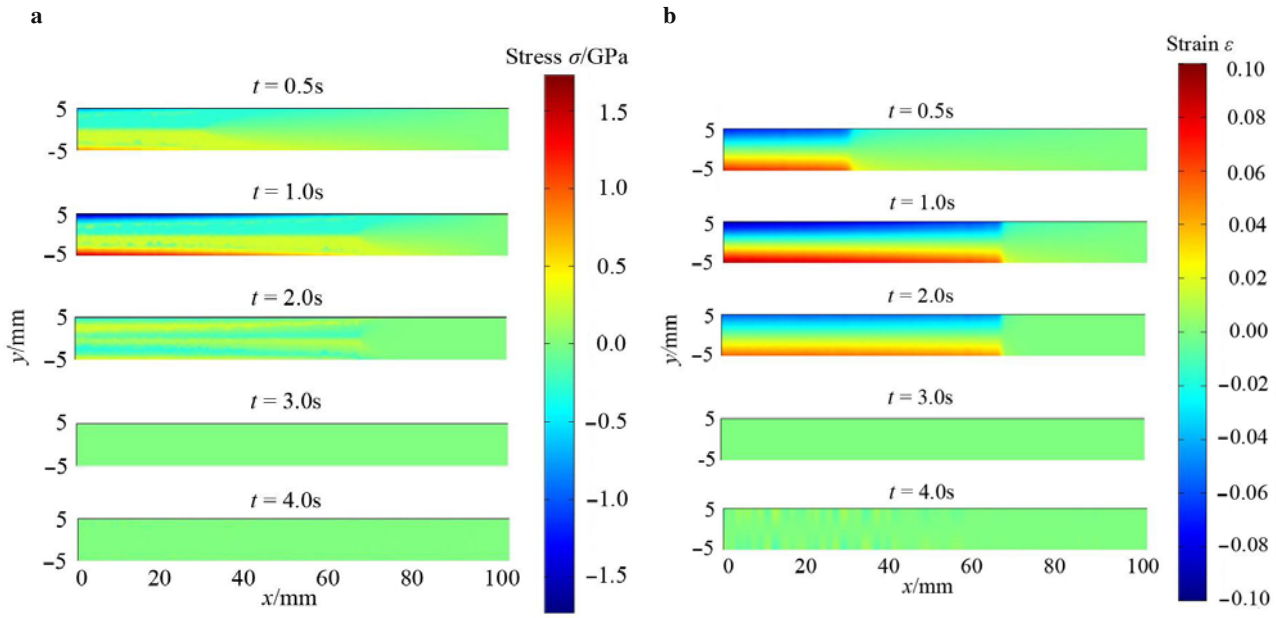

Fig. 3 Shape memory effect contour plot of SMA beam bending: **a** Stress; **b** Strain; **c** Phase fraction x_+; **d** Phase fraction x_-

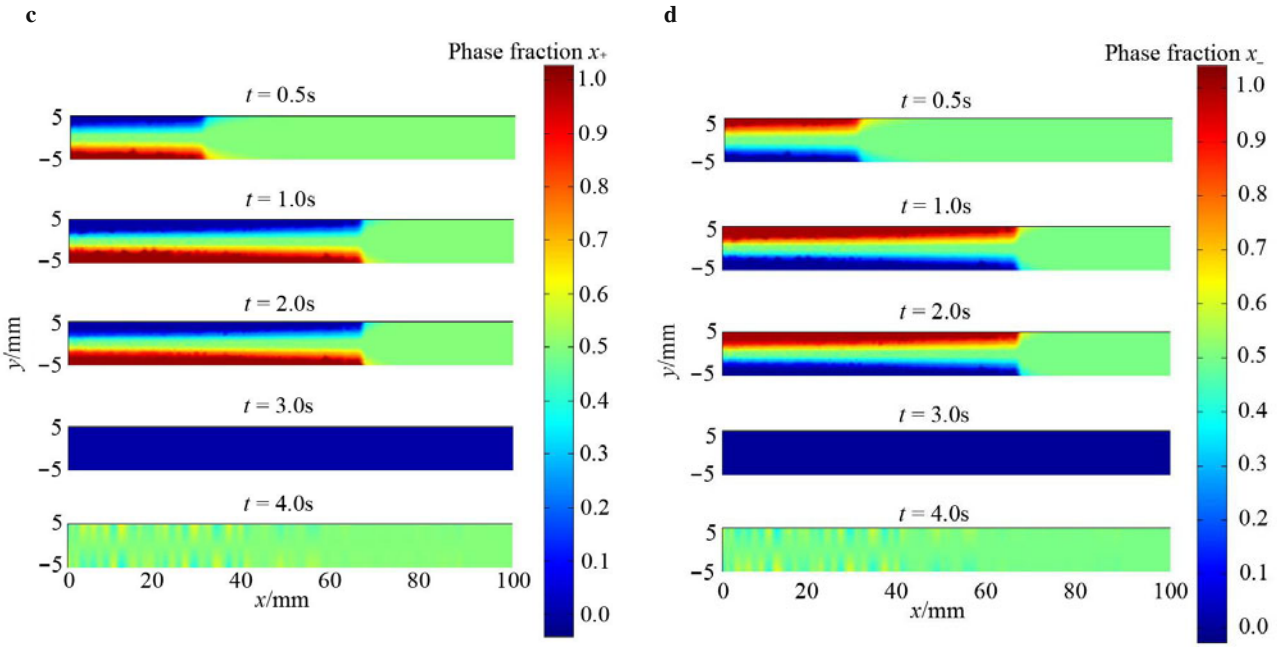

Fig. 3 Shape memory effect contour plot of SMA beam bending: **a** Stress; **b** Strain; **c** Phase fraction x_+; **d** Phase fraction x_- (continued)

5.2 Thermal boundary condition effect

In this part, we study the super-elastic behaviors of the SMA cantilever under different thermal boundary conditions: (1) constant temperature $T(\Omega) = T_0$; (2) adiabatic boundary conditions $\partial T/\partial x(\partial\Omega, t) = \partial T/\partial y(\partial\Omega, t) = 0$; (3) fixed temperature boundary conditions $T(\partial\Omega, t) = T_0$. The ambient temperature is $T_0 = 333$ K.

First, we assume the SMA beam has a constant temperature, which means the temperature field of the beam stays constant at the ambient temperature. The applied tip force $F(t)$ is given in Fig. 4a (top). The SMA material is in the austenite state at this temperature under zero mechanical loading. So the simulation starts with the initial phase fractions as $x_+ = x_- = 0$. Figure 4a (bottom) shows the displacement response. The corresponding force displacement diagram is shown in Fig. 4b, which illustrated the super-elastic behavior of the SMA beam bending with gradual phase transformation at 333 K. The SMA beam is able to recover large deformation after unloading. This qualitatively matches the result reported by Auricchio and Sacco [29].

The inhomogeneous phase transformation of the SMA beam bending is illustrated in the contour plots of the stress, strain and phase fractions during the loading and unloading process in Fig. 5. Upon loading, the area below the neutral axis, subject to tensile stresses, transforms from A to martensite M_+ and the area above the neutral axis subject to compression stresses which transforms from A to martensite M_- together result in a large deflection of the SMA beam as shown in Fig. 4. Upon unloading, the SMA beam transforms back into austenite A and recovers its original shape. During the loading process, the outer parts of the clamped end reach the transform stress σ_A first and the phase transformation starts there and develops longitudinally and transversely. The reverse process occurs during the unloading process.

For the SMA beam bending under adiabatic boundary conditions, $\partial T/\partial x(\partial\Omega, t) = \partial T/\partial y(\partial\Omega, t) = 0$, the same applied force as before, see Fig. 4a. There is no heat transfer between the SMA material and the air. The strain and stress process is similar to the above. Figure 6 shows the temperature contour of the SMA beam. Upon loading, the latent heat is released from where the phase transformation happens and conducted longitudinally and transversely which makes the local temperature quite high. The neighboring area needs higher stress to overcome the energy barrier in order to implement phase transformation. This means the phase transformation is delayed by the thermomechanical effect which results in lower deflection under the same applied force, see Fig. 7. Upon unloading, the SMA beam transforms back into austenite A and recovers to its original shape. And the phase transformation area absorbs heat which results in lower local temperature.

For fixed temperature boundary conditions, $T(\partial\Omega, t) = T_0$, the same force is applied to the beam. In this case, the heat transfer is very efficient between the SMA materials and ambient. The temperature contour plot is shown in Fig. 8 during the loading and unloading process. The beam has similar latent heat release and heat absorbing upon loading except in the beam boundary area. The beam also releases heat to the ambient and absorbs heat from the ambient. As a result, the phase transformation area has a higher temperature than the isothermal boundary simulation but lower than

the adiabatic boundary condition case. The maximum deflection is between the two simulations above, see Fig. 7.

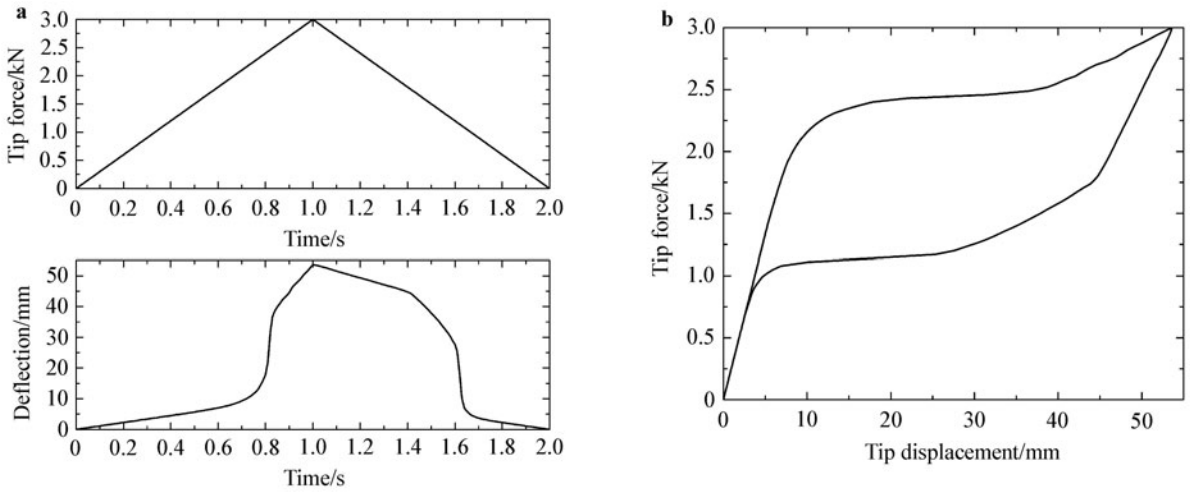

Fig. 4 Super-elastic behavior of SMA beam bending: **a** Applied tip force and displacement response vs. time; **b** Tip force vs. tip displacement

5.3 Load rate effect

For better comparison, the same simulation parameters and fixed temperature boundary conditions are used. The process of the applied force is extended to 20 s. The load rate drops from 3 kN/s to 0.3 kN/s. The temperature contour plots under the loading and unloading process are shown in Fig. 9. The time points become 8 s, 9 s, 10 s, 16 s and 17 s. Comparing this with a higher load rate, see Fig. 8, the heat is conducted to a wider area. The highest temperature is lower than that in the high load rate case. And the maximum deflection is between a high load rate under a fixed temperature boundary condition simulation and isothermal simulation, see Fig. 7. This load rate effect matches the result which was reported in Ref. [30].

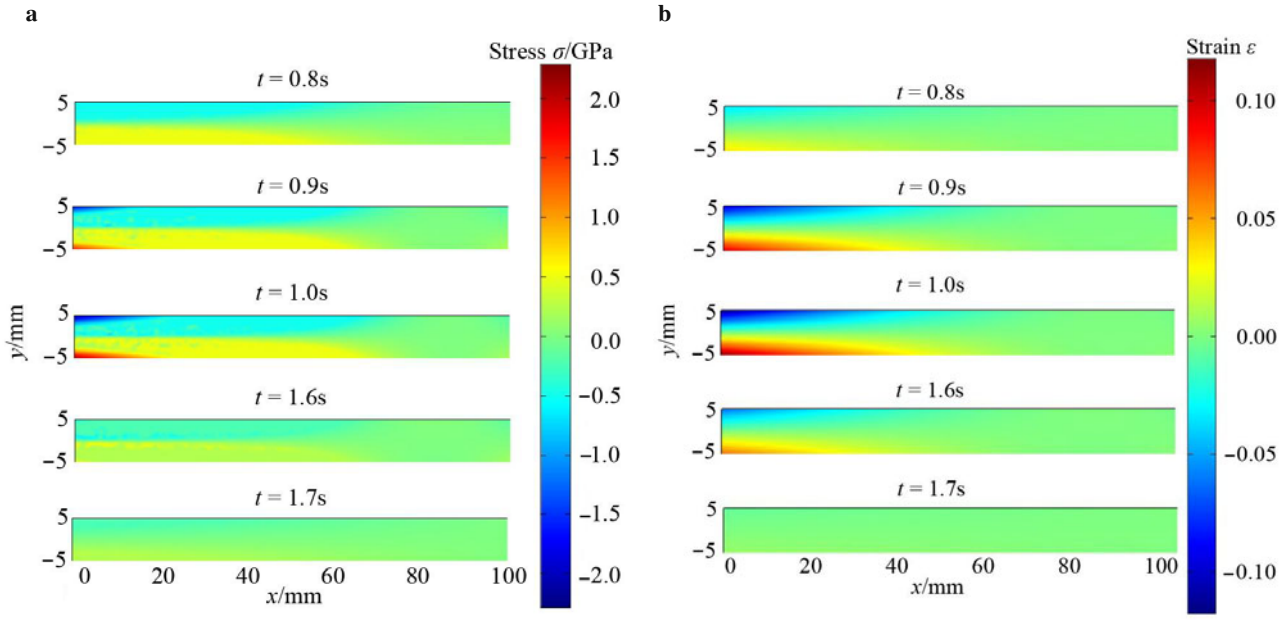

Fig. 5 Contour plot of super-elastic SMA beam bending: **a** Stress; **b** Strain; **c** Phase fraction x_+; **d** Phase fraction x_-

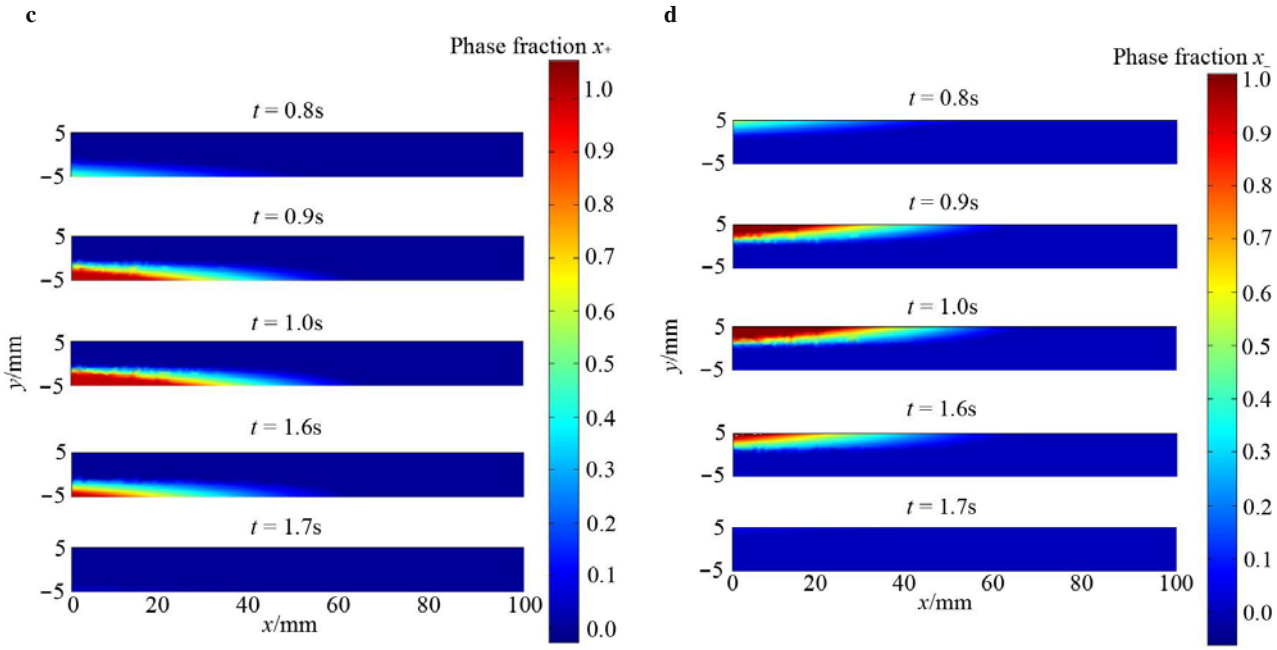

Fig. 5 Contour plot of super-elastic SMA beam bending: **a** Stress; **b** Strain; **c** Phase fraction x_+; **d** Phase fraction x_- (continued)

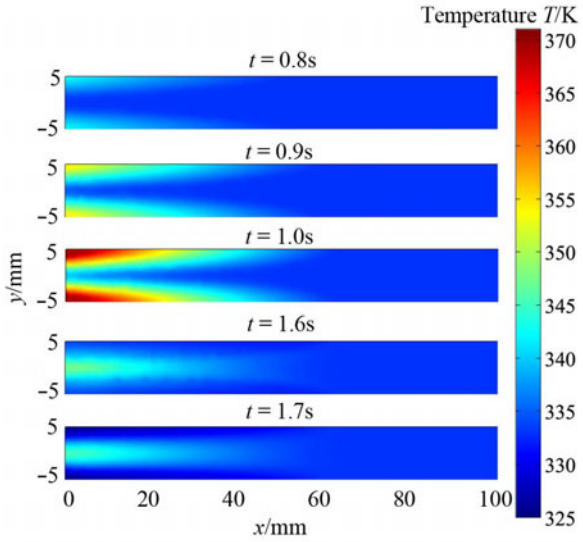

Fig. 6 Temperature contour plot under adiabatic boundary conditions

6 Conclusions

A thermomechanical model of a shape memory alloy beam bending under tip force loading is implemented in finite element codes. The constitutive model is a one dimensional model which is based on free energy and motivated by statistical thermodynamics. The implementation of the beam is based on the small deformation Euler–Bernoulli beam theory. The simulations represent both the shape memory effect and super-elastic behavior. The stress, strain and phase transformation developing process are illustrated. Two severe boundary conditions: adiabatic and fixed temperature boundary conditions were implemented. The load rate effect can also be captured. These simulations illustrated the thermo-mechanical coupling effect in the beam bending problem. This is an efficient tool to study thermo-mechanical smart materials such as SMA and to predict the behavior of the adaptive structure.

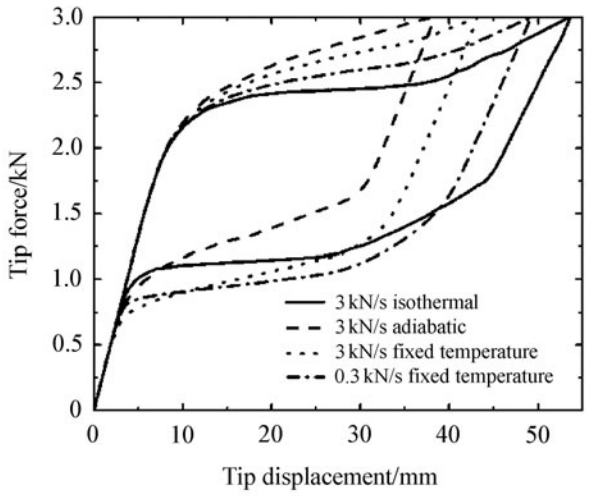

Fig. 7 Force vs. deflection

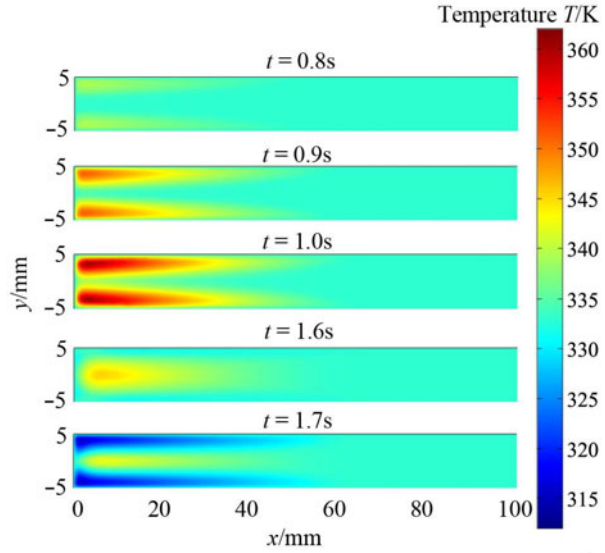

Fig. 8 Temperature contour plot under fixed temperature boundary conditions

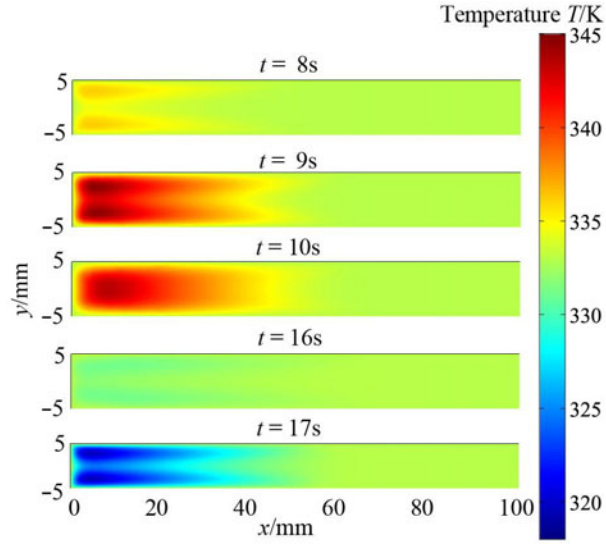

Fig. 9 Temperature contour plot under fixed temperature boundary conditions (low load rate)

References

1 Krulevitch, P., Lee, A.P., Ramsey, P.B. et al.: Thin film shape memory alloy microactuators. Journal of Microelectromechanical Systems **5**(4), 270–282 (1996)

2 Kohl, M., Krevet, B., Just, B.: SMA microgripper system. Sensors and Actuators A: Physical **97-98**, 646–652 (2002)

3 Xu, D., Wang, L., Ding G. et al.: Characteristics and fabrication of NiTi/Si diaphragm micropump. Sensors and Actuators A: Physical **93**(1), 87–92 (2002)

4 Ishida, A., Sato, M.,Yoshikawa W. et al.: Bimorph-type microactuator using TiNi shape-memory thin film. Material Science Forum **394-395**, 487–490 (2001)

5 Kohl, M., Brugger, D., Ohtsuka D. et al.: A novel actuation mechanism on the basis of ferromagnetic SMA thin films. Sensors and Actuators A: Physical **114**(2-3), 445–450 (2004)

6 Namazu T., Tashiro Y., Inoue S.: Ti–Ni shape memory alloy film-actuated microstructures for a MEMS probe card. Journal of Micromechanics and Microengineering. **17**(1), 154–162 (2007)

7 Tanaka K., NagaKi S.: A thermomechanical description of materials with internalvariables in the process of phase transition. Archive of Applied Mechanics **51**(5), 287–299 (1982)

8 Liang, C., Rogers, C.A.: One-dimensional thermomechanical constitutive relations for shape memory materials. Journal of Intelligent Material System and Structures **1**(2), 207–234 (1990)

9 Ahluwalia, R., Lookman, T., Saxena, A. et al.: Landau theory for shape memory polycrystals. Acta Materialia **52**(1), 209–218 (2004)

10 Elliott, R.S., Shaw, J.A., Triantafyllidis, N.: Stability of crystalline solids—II: application to temperature-induced martensitic phase transformations in a bi-atomic crystal. Journal of Mechanics and Physics of Solids **54**(1), 193–232 (2006)

11 Huang, X., Ackland, G.J., Rabe, K.M.: Crystal structures and shape-memory behaviour of NiTi. Nature Materials **2**(5), 307–311 (2003)

12 Ivshin, Y., Pence, T.J.: A thermomechanical model for a one variant shape memory material. Journal of Intelligent Materials System and Structures **5**(4), 455–473 (1994)

13 Amalraj, J.J., Bhattacharyya, A., Faulkner, M.G.: Finite-element modeling of phase transformation in shape memory alloy wires with variable material properties. Smart Mater. Struct. **9**(5), 622–631 (2000)

14 Meier, H., Oelschlaeger, L.: Numerical thermomechanical modeling of shape memory alloy wires. Materials Science and Engineering A **378**(1-2), 484–489 (2004)

15 Tsoi, K.A., Schrooten, J., Stalmans, R.: Part I. Thermomechanical characteristics of shape memory alloys. Materials Science and Engineering A **368**(1-2), 286–298 (2004)

16 Müller, C., Bruhns, O.T.: A thermodynamic finite-strain model for pseudoelastic shape memory alloys. International Journal of Plasticity **22**(9), 1658–1682 (2006)

17 Azadi, B., Rajapakse, R.K.N.D., Maijer, D.M.: One-dimensional thermomechanical model for dynamic pseudoelastic response of shape memory alloys. Smart Mater. Struct. **15**(4), 996–1008 (2006)

18 Zhu, S., Zhang, Y.: A thermomechanical constitutive model for superelastic SMA wire with strain-rate dependence. Smart Mater. Struct. **16**(5), 1696–1707 (2007)

19 Shaw, J.A.: A thermomechanical model for a 1D shape memory alloy wire with propagating instabilities. International Journal of Solids and Structures **39**(5), 1275–1305 (2002)

20 Iadicola, M.A., Shaw, J.A.: Rate and thermal sensitivities of unstable transformation behavior in a shape memory alloy. International Journal of Plasticity **20**(4-5), 577–605 (2004)

21 Chang, B.C., Shaw, J.A., Iadicola, M.A.: Thermodynamics of shape memory alloy wire: modeling, experiments, and application. Continuum Mech. Thermodyn. **18**(1-2), 83–118 (2006)

22 Shaw, J.A., Churchill, C.B.: A reduced-order thermomechanical model and analytical solution for uniaxial shape memory alloy wire actuators. Smart Mater. Struct. **18**(6), 065001–065022 (2009)

23 Achenbach, M., Müller, I.: Simulation of material behavior of alloys with shape memory. Arch Mech. **37**(6), 573–585 (1985)
24 Achenbach, M.: A model for an alloy with shape memory. International Journal of Plasticity **5**(4), 371–395 (1989)
25 Seelecke, S., Müller, I.: Shape memory alloy actuators in smart structures-modeling and simulation. Appl. Mech. Rev. **57**(1), 23–46 (2004)
26 Thiebaud, F., Collet, M., Foltete, E. et al.: Implementation of a multi-axial pseudoelastic model to predict the dynamic behavior of shape memory alloys. Smart Mater. Struct. **16**(4), 935–947(2007)
27 Rahman, M.A., Kowser, M.A.: Nonlinear analysis of cantilever shape memory alloy beams of variable cross section. Smart Mater. Struct. **16**(2), 531–540 (2007)
28 Yang, S., Seelecke, S., Li, Q.: Finite element analysis of SMA beam bending using COMSOL. Proc. of SPIE **7289**, (2009) doi: 10.1117/12.816714
29 Auricchio, F., Sacco, E.: A temperature-dependent beam for shape memory alloys: constitutive modelling, finite element implemenation and numerical simulations. Computer Methods in Applied Mechanics Engineering **174**(1-2), 171–190 (1999)
30 Auricchio, F., Sacco, E.: Thermo-mechanical modeling of a superelastic shape-memory wire under cyclic stretching-bending loadings. International Journal of Solid and Structures **38**(34-35), 6123–6145 (2001)